THE RELATIONSHIP BETWEEN HARD AND SOFT X-RAY BURSTS OBSERVED BY OSO 7

DAYTON W. DATLOWE
University of California, San Diego, La Jolla, Calif., U.S.A.

Abstract. Solar X-rays in the energy range 1–100 keV originate in hot plasmas and streams of energetic electrons in solar flares, and since these phenomena may represent a significant fraction of the energy in a flare, an understanding of them is important for any flare theory. This paper presents the results of the University of California, San Diego, solar X-ray instrument on the OSO-7 satellite. Study of the time evolution of the emission measure in a typical burst indicates that the growth of soft X-ray emission is due to the addition of new hot material to the flare plasma, and the study of the time evolution of the temperature of the plasma indicates that conduction is the dominant cooling mechanism. Comparison of the hard (10–100 keV) and soft (5–10 keV) data indicates that the main heat input to the flare plasma is not collisions by the electrons which make the hard X-rays. The fraction of soft X-ray bursts observed by the instrument which also have a detectable hard X-ray component is $\frac{2}{3}$; this result is the same for bursts which occured near the center of the disk ($\theta < 60°$) and for those bursts believed to have been partly occulted by the limb, indicating that hard X-ray emission comes at least part from high in the corona. For a sample of 62 hard X-ray bursts which occurred near or beyond the limb, the spectral index of the hard X-ray power law was significantly larger, as compared with the spectra of a comparable number which occurred at solar longitudes less than 60°.

1. Introduction

This paper is a review of the observations made by the University of California, San Diego, solar X-ray instrument on the OSO-7 satellite. The instrument is the first to observe simultaneously both the hard and soft components of an X-ray burst in separate detector systems; thus it is uniquely suited to examine the relationship between the two spectral components. Solar X-rays give information about hot plasmas and streams of energetic electrons in solar flares, and since the amount of energy in these phenomena are comparable to the total energy of the flare, understanding their origin is of considerable importance for any flare theory. This paper will explore the relationship between the hard and soft X-ray components and what can be learned about the physics of solar flares from a detailed comparison of them.

II. Soft X-Rays

Soft X-rays in the 4–10 keV range observed by the instrument come from hot (10^7 K) plasmas associated with solar flares. Previous measurements of the soft X-ray continuum have been described in White (1964), Neupert (1967), Hudson *et al.* (1969), Culhane and Phillips (1970), Teske (1971), Kahler *et al.* (1970) and Valnicek *et al.* (1973). The only previous systematic study of a number of bursts was by Horan (1971), uing 17 large bursts observed by a broad band counter on the OSO-4 satellite. Little observational effort has been directed toward the statistical study of the temperatures and emission measures of bursts, nor has much effort been directed toward direct correlative observations with hard X-ray bursts. The OSO-7 observations have

Sharad R. Kane (ed.), Solar Gamma-, X-, and EUV Radiation, 191–208.

made possible the first systematic study of a large number of bursts; the set contains 197 events which occurred between October, 1971, and June, 1972, over which time about 40% data coverage was obtained.

The OSO-7 soft X-ray detector (Datlowe *et al.*, 1974a) consists of a 2.54 cm diameter proportional counter with a $Xe(CO_2)$ fill. Pulses from the detector are analyzed into channels approximately 1.4 keV wide. A thermal spectrum is fitted to the channels from 5.1–10.6 keV to determine a temperature and emission measure, such that when the spectrum is folded through the detector response the best fit to the pulse height distribution is obtained. The thermal spectrum is approximated by the formula of Culhane and Acton (1970), which takes into account both free-free and free-bound emission; line emission, particularly from iron at 6.65 keV, is neglected. The estimated total systematic error in the temperature is 2×10^6 K, and in the emission measure a factor of 2.

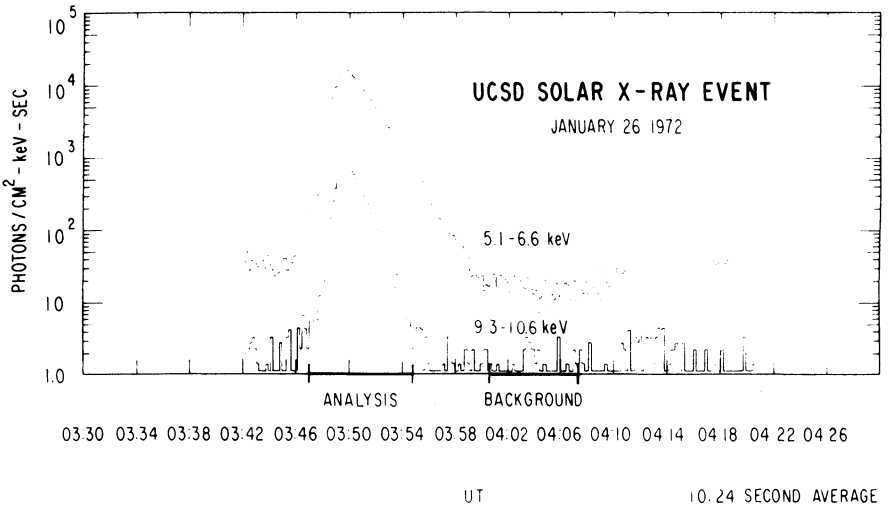

Fig. 1. Soft X-ray flux from a −N flare at 0346 UT on 1972, January 26. The two energy channels shown are 5.1–6.6 and 9.3–10.6 keV. The time over which the analysis was performed and the time used to estimate the background are indicated by heavy lines at the bottom of the figure. Each point represents 10.24 s of data.

A typical burst observed by the OSO-7 solar X-ray instrument is shown in Figure 1. The event occurred in 1972, January 26 at 0348 UT and was associated with a −N subflare. The figure shows the 5.1–6.6 keV and 9.3 to 10.6 keV channels. The flux shows a rapid rise, lasting for about 2 min, and a slow decay lasting for about 10 min. The time intervals used for the spectral analysis and for the background estimate are indicated by heavy lines at the bottom of the figure.

Although solar X-ray bursts are sometimes characterized by a single temperature and emission measure pair, these quantities evolve throughout the course of an event. Figure 2 shows this evolution for the sample burst, where each point represents a

30.72 s average. The maximum temperature, 15×10^6 K, was achieved early in the burst and thereafter the temperature declined slowly. The emission measure grew exponentially for about 2 min, reaching a maximum value of 10^{49} cm^{-3}. For an assumed density of 5×10^{10} cm^{-3} (Hudson and Ohki, 1972), the thermal energy in the hot flare plasma is 1×10^{30} erg.

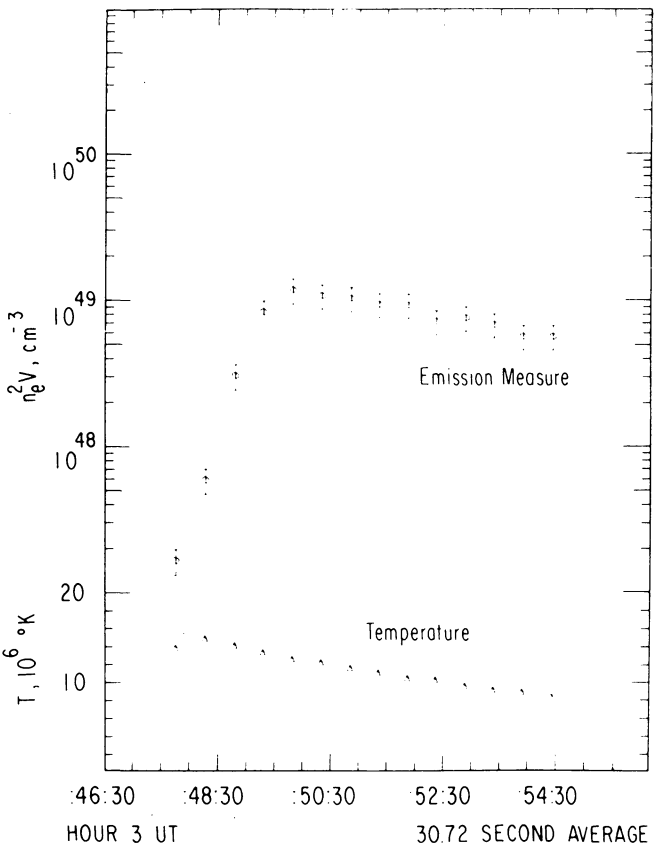

Fig. 2. The temperature and emission measure for the burst shown in Figure 1. The temperature (triangles) is plotted on a linear scale and the emission measure (circles) is plotted on a logarithmic scale. Error bars shown for the emission measure represent an assumed 20% systematic error, as well as the statistical error.

This kind of analysis was carried out systematically for all bursts during the observing period, for which the flux in the 5.1–6.6 keV channel exceeded 10^3 photons $(\text{cm}^2 \text{ s keV})^{-1}$ and for which there was sufficient data coverage. In all, 197 bursts were analyzed, 17 associated with class 1 flares, 135 associated with subflares, and the remainder were unreported in *Solar Geophysical Data*. The evolution of the emission measure was largely the same in each case. There is a rising phase which is quasi-exponential and which lasts for a few minutes. The distribution of risetimes is shown in Figure 3c, showing that half of the risetimes are between 30 and 100 s. The figure

https://doi.org/10.1017/S0074180900071692 Published online by Cambridge University Press

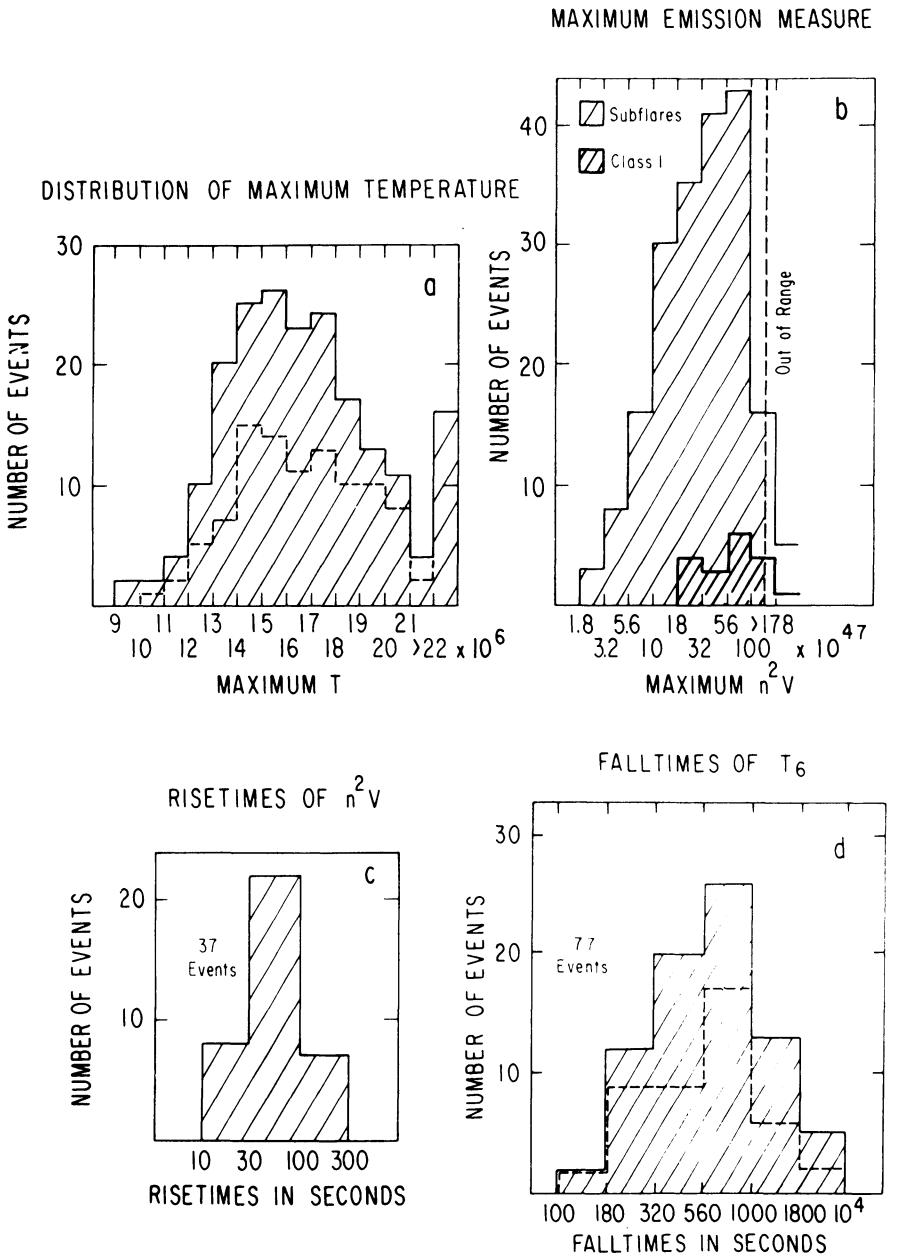

Fig. 3. Distributions of parameters characterizing soft X-ray events from 197 examples. (a) Distribution of maximum temperature for an individual burst. (b) Distribution of maximum emission measure. Importance I flares are shown separately, and instrument saturation causes the cutoff for large bursts. (c) Distribution of risetimes of emission measure for the 37 cases in which an exponential growth rate gave a good fit to the data. (d) Distribution of falltimes of temperature for 77 subflares in which an exponential decay gave a good fit to the data. Events below the dotted lines in (a) and (d) are associated with analyzed hard X-ray bursts.

https://doi.org/10.1017/S0074180900071692 Published online by Cambridge University Press

contains only 37 events because a good fit to an exponential was required in preparing the distribution; including events with deviations from an exponential would produce a similar distribution. The median value of the peak emission measure is 30×10^{47} cm^{-3}, and for the bursts in this sample the maximum emission measure usually fell between 10 and 100×10^{47} cm^{-3}. The median temperature at the time of peak emission measure was 11×10^6 K.

The temperature evolution is somewhat different. The maximum temperature is reached early in the event; frequently the observations are consistent with $dT/dt < 0$ throughout the event. The median decay time for the temperature is 600 s, and the distribution of decay times is shown in Figure 3d. The distribution of maximum temperatures is shown in Figure 3a. This latter distribution is relatively flat for temperatures of $13 \leqslant T_{max} \leqslant 19 \times 10^6$ K, and the median value is 17×10^6K. Since the time of maximum temperature is early in the burst, the emission measure at that time is much smaller than the peak value, and in most of these events it lies between 10^{47} cm^{-3} and 5×10^{47} cm^{-3}.

Inference about the cooling mechanism of the hot flare plasma can be made from a study of the cooling time. The two principal cooling mechanisms (Culhane *et al.*, 1970; Roy and Datlowe, 1974) which must be considered are radiation and conduction. These possibilities can be examined on the assumption that the heat flow is determined by changes in temperature only; this is probably valid during the decay phase but, as well be shown later, cannot be valid during the rising phase of the burst. For free-free radiative cooling, the decay time is related to the temperature by $\tau \propto T^{1/2}$. Free-bound and line emission can be taken into account (Culhane *et al.*, 1970) but this does not make a significant change in the numerical value of the exponent in the present context. Conductive cooling on the other hand predicts a relationship between the cooling time and the temperature of the form $\tau \propto T^{-2.5}$. It can be seen that there should be a correlation between the temperature and the cooling time, and that a positive correlation would favor radiative cooling while an anticorrelation would favor conductive cooling. This correlation has been tested using both T_{max} and the average temperature over the time interval used to determine the cooling time. The result is that the sign of the correlation is negative although it is not a strong correlation. This favors conduction as the dominant cooling mechanism in these subflares.

Many of the soft X-ray bursts were accompanied by hard X-ray bursts simultaneously observed by the instrument. To see if there is a correlation between the soft X-ray parameters and the presence or absence of an accompanying hard X-ray burst, Figure 3a shows the maximum temperatures for bursts with a hard X-ray component *below* the dotted line. The distribution is substantially the same for bursts above and below the line. For emission measures, similar results are obtained except that a greater fraction of bursts with large emission measures have hard components, possibly a threshold effect. In general, when the distribution of soft X-ray parameters for those bursts with a hard X-ray component is compared to the same distribution for those in which no hard component was detected, there is no important difference.

These observations place a number of constraints on the physics of the hot flare plasma and its heating mechanism. The amount of energy stored in the hot plasma may be comparable to the total energy of the flare and thus its origin is very important for flare theory. The X-ray data make it possible to estimate the energy content of the plasma and to observe its time variations.

The key experimental facts are that the temperature and emission measure appear to evolve independently, inasmuch as the maximum of one is not reflected in the maximum of the other, and that the emission measure typically grows by a factor of 100 throughout a burst while the temperature steadily declines. The following are possible models for the evolution of the plasma:

(1) A fixed amount of plasma is directly heated by nonthermal electrons. The emission measure stays constant and the temperature increases in proportion to the energy input.

(2) A constant amount of plasma is compressed by a factor of 100. In this case the number of particles nV stays the same but the emission measure n^2V increases.

(3) New plasma is injected into a relatively constant volume, such as a pre-existing arch system. The amount of matter in the volume nV, and the plasma thermal energy $3\,nVkT$ each increase by a factor of 10, but the emission measure n^2V increases by a factor of 100.

(4) The volume of the emission region and the amount of matter and thermal energy in it grow by a factor of 100, while the density stays relatively constant. This might occur if successive flux tubes are heated to temperatures of 10^7 K but no mass motion occurs.

Case number 1 can be eliminated immediately, since it predicts precisely the converse of the observed evolutions. The independence of the temperature and the emission measure evolution rules out case 2; during the growth phase the heat of compression must be removed from the plasma, since the temperature is slowly falling. Once the compression is complete the same cooling mechanism would cause a rapid temperature drop in the plasma, which is not observed. In fact, the transition from the growth phase of the emission measure to the decay phase is not detectable in the temperature evolution.

Cases 3 and 4 are both consistent with the OSO-7 observations. In both cases new plasma is added to the soft X-ray emitting region. While the two possibilities cannot be distinguished on the basis of the present data alone, it should be noted that case 3 (constant volume) involves the addition of significantly less energy to the plasma than case 4 (constant density). Spatially resolved or imaging soft X-ray experiments can distinguish between the two models.

A second consequence of the independence of the temperature and emission measure evolution is that heat flows cannot be inferred from temperature changes alone. The new matter which is added to the flare plasma brings in heat, while from the declining temperature one might infer that heat is flowing out of the region. Thus the question of conductive cooling versus radiative cooling must be replaced by a realistic model of the total thermal evolution of the plasma.

III. Hard X-Rays

Hard solar X-rays come from bremsstrahlung due to collisions of 10–100 keV electrons with the solar atmosphere. The spectrum of this component is characteristically a power law, and its duration is typically 1 minute for bursts associated with subflares, although variability in the flux on time scales of the order of 1 second has been observed (Frost, 1969). Several satellite experiments have observed hard solar X-radiation since its discovery by Peterson and Winckler (1959); a good historical summary will be found in Kane (1974). The OSO-7 observations (Datlowe *et al.*, 1974b) have provided the first systematic study of hard solar X-ray burst morphology.

The hard X-ray detector on the OSO-7 solar X-ray instrument consists of a 9.57 cm^2 Na I(Tl) scintillation counter which is actively shielded by a Cs I(Na) collimator. The entrance window consists of 0.041 g cm^{-2} of aluminum. Pulses from the detector are analyzed into 9 logarithmically spaced channels from 10.6–323 keV. In the analysis a power law X-ray spectrum is fitted to the hard X-ray pulse height distribution in the same way that a thermal spectrum is fitted to the soft X-ray data. Since the photons which the instrument observes are typically at energies of 20 keV, spectra are normally referred to that energy, given in the form of $A(E/20)^{-\gamma}$ photons $(cm^2\ s\ keV)^{-1}$; normalization at 1 keV is sensitive to small errors in the slope and gives less reliable results.

The behavior of a typical event is shown in Figure 4, which gives the soft

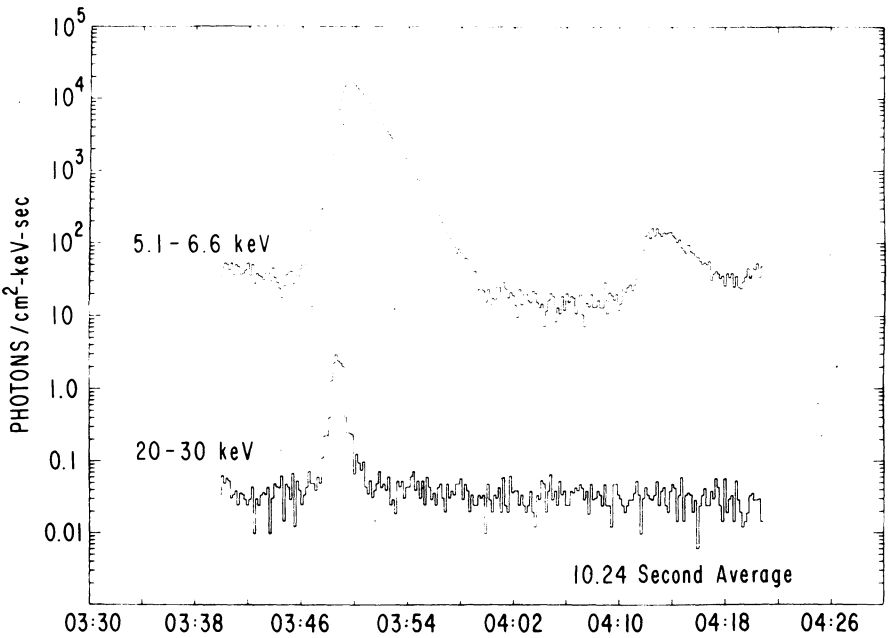

Fig. 4. Hard and soft X-ray fluxes from the sample event, Figure 1. The lower trace gives the 20–30 keV channel of the Na I (Tl) detector, representative of the hard X-ray flux. For comparison, the 5.1–6.6 keV channel of the soft X-ray detector is shown again in the upper trace. Hard X-ray analysis was carried out from 034731 to 034924 UT.

https://doi.org/10.1017/S0074180900071692 Published online by Cambridge University Press

(5.1–6.6 keV) and hard (20–30 keV) fluxes for the 1972, January 26 sample event. The soft and hard X-ray components have comparable time histories during the rising phase, with the greatest flux increase in both channels occurring in the same data sample. The hard X-ray flux peaks earlier and dies away rapidly compared to the soft X-ray flux. This figure shows clearly the ability of the OSO-7 solar X-ray instrument to separate the hard and soft components of an X-ray burst. The evolutions of the spectral parameters A and γ are shown in Figure 5. Each data point represents a 10.24 s average, the maximum time resolution of the instrument. The maximum value of the 20 keV flux A was ≈ 4 photons $(\text{cm}^2\ \text{s keV})^{-1}$ and the flux remained at this value for five data samples, 51 s. The hardest individual spectrum, $\gamma = 2.6$, occurred at 20 keV flux maximum, and the average spectral index was $\bar{\gamma} = 3.1$.

This kind of analysis has been carried out for 123 bursts. Two-thirds of the bursts observed by the proportional counter with peak fluxes greater than 10^3 photons

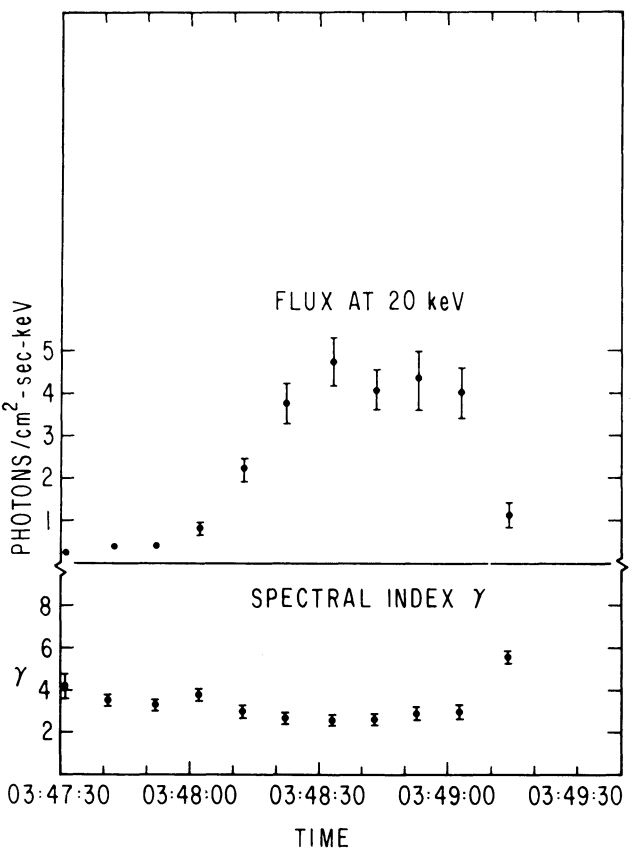

Fig. 5. Hard X-ray emission parameters for the sample event in 1972, January 26. The spectral index γ and the flux at 20 keV are plotted on a linear scale. Statistical errors in the flux are shown, while for the spectral index the error shown is the combination of the statistical error and an assumed systematic error of $\Delta\gamma = 0.3$.

https://doi.org/10.1017/S0074180900071692 Published online by Cambridge University Press

$(cm^2\ s\ keV)^{-1}$ at 5 keV also had a detectable hard X-ray component at 20 keV. Eighty percent of these events reached a maximum flux $A_m > 0.2$ photons $(cm^2\ s\ keV)^{-1}$ and could be analyzed, while for the remainder the flux was too small to fit a spectrum. The analysis yielded a measurement of the peak 20 keV flux, the spectral index at maximum, the average spectral index, and the duration of the burst.

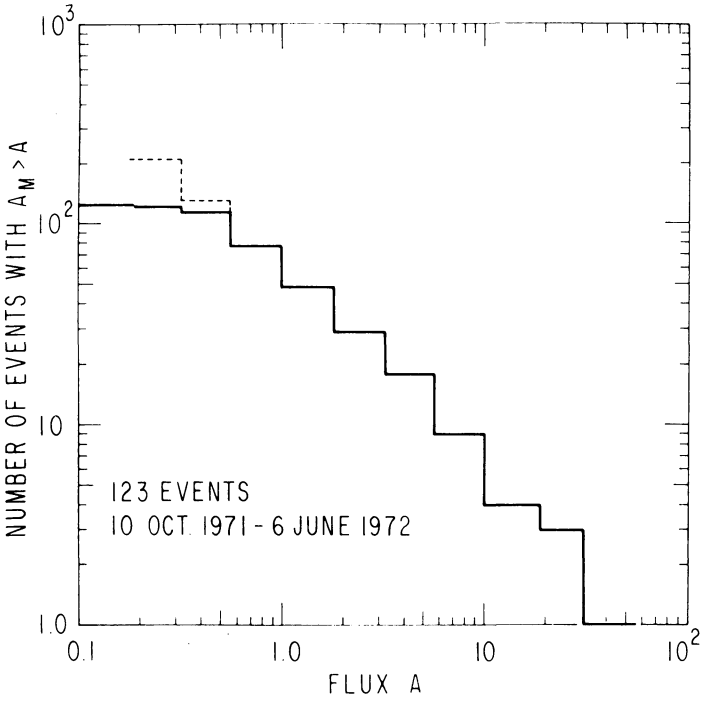

Fig. 6. Integral distribution of frequency of events vs peak hard X-ray flux. The dotted line represents an extrapolation of this distribution until N equals the number of soft X-ray bursts observed. If the distribution continued smoothly down to $A = 0.2$ photons $(cm^2\ s\ keV)^{-1}$ then the number of hard and soft X-ray bursts in the sample would be the same.

The distribution of peak hard X-ray flux at 20 keV, A_m, is shown in Figure 6. The distribution is relatively smooth between $1 < A_m < 10$ photons $(cm^2\ s\ keV)^{-1}$ and flattens below a flux of 0.5. This flattening appears to be a threshold effect; if this is the case, then the fraction of soft X-ray bursts with a hard X-ray component may be greater than $\frac{2}{3}$. Nonetheless, it does appear that there is a distinct class of soft X-ray bursts with large fluxes which do not exhibit any hard X-ray emission.

The quantity γ_m denotes the spectral index in the 10.24-s data sample which had the largest 20 keV flux, A_m, in a particular burst. Figure 7a shows the distribution of the frequency of occurrence of γ_m. The median value is $\gamma_m = 4.0$ and values outside the range 2.5–6.0 rarely occur. The distribution of the average spectral index $\bar{\gamma}$ computed as described in Datlowe *et al.* (1974b), is shown in Figure 7b. The median is $\gamma = 4.6$ and

https://doi.org/10.1017/S0074180900071692 Published online by Cambridge University Press

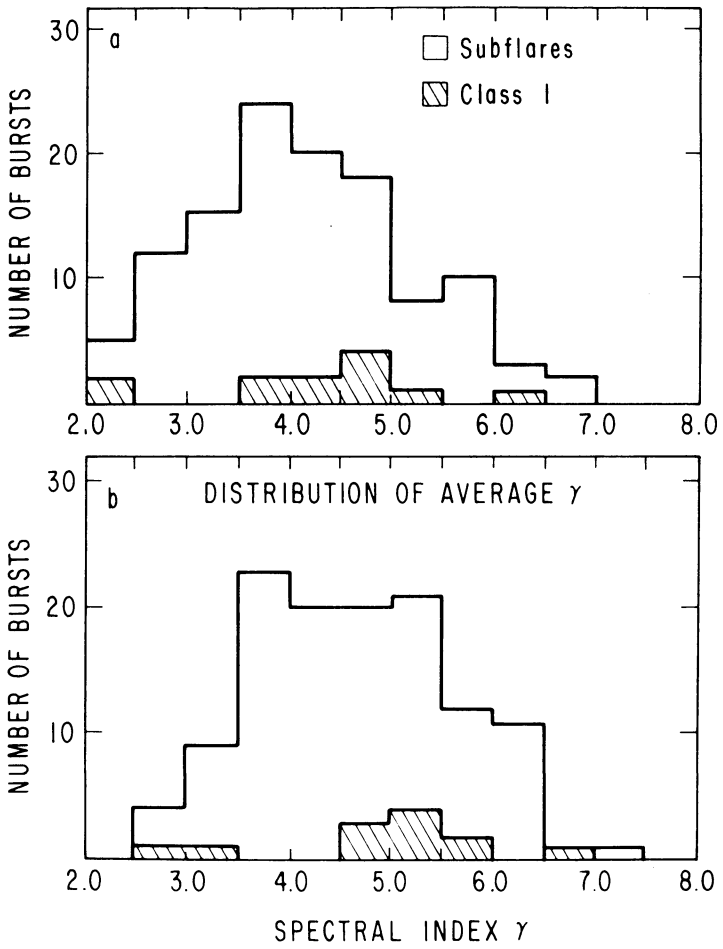

Fig. 7. Distributions of the frequency of occurrence of the spectral indices for 123 bursts. (a) The spectral index at the time of maximum 20 keV flux, γ_m. (b) Average spectral index, $\bar{\gamma}$, computed as described in Datlowe *et al.* (1974). Events associated with importance 1 flares are crosshatched.

the width of the distribution is $\sigma_\gamma = 1.0$. The two spectral indices are highly correlated and related by $\bar{\gamma} \approx \gamma_m + 0.5$.

Within a given burst, individual samples of the spectral index γ are highly correlated. Kane and Anderson (1970) found in their OGO-5 data that the spectral index tended to vary from soft to hard to soft as the burst evolved. The sample burst in Figure 5 also shows this kind of evolution. However, in the OSO-7 data a much more common case is an evolution in which the spectral index becomes progressively larger with each data sample; thus the spectrum softens or stays nearly constant throughout the course of the burst. There is no correlation between the spectral index and the flux in an individual sample using 1111 individual spectral in the OSO-7 data, the coefficient of correlation between A and γ is 0.04.

https://doi.org/10.1017/S0074180900071692 Published online by Cambridge University Press

Finally, the experiment yields statistics on the durations of hard X-ray bursts, the length of time that a given burst remains above the flux threshold of 0.1 photons $(\text{cm}^2\,\text{s}\,\text{keV})^{-1}$ at 20 keV. Durations observed by the instrument range from the shortest time resolution of the instrument, 10.24 s, to 800 s. For the subflares the median duration is 92 s, while for bursts associated with class 1 flares the median is 50% longer. There is a weak correlation between burst size and duration in the sense that events with a larger peak flux A_m tend to last longer. These durations are notably longer than those of Kane and Anderson (1970) but are in agreement with the observations of Frost and Dennis (1971).

IV. Burst Energetics

From hard X-ray spectra it is possible to estimate the energy of the nonthermal electrons in the X-ray emitting region. The X-ray spectrum depends only on the instantaneous electron spectrum, $N(E)$, but the total collision losses depend on the spectrum of the accelerated electrons. In the thin target case electrons predominantly escape, so that the accelerated and instantaneous spectra are essentially the same; in the thick target case electrons lose all of their energy to collisions, and the injected spectrum $F(E)$ differs from $N(E)$. In the present analysis the formulae of Brown (1972) are used as the model for X-ray emission. Slightly different results would be obtained under different assumptions about the chemical composition of the X-ray region, about inhomogeneities in the X-ray region, and about the directivity of the radiation due to electron streaming. In all of the OSO-7 solar X-ray calculations, it is assumed that the electron spectrum is a power law above 20 keV, corresponding to the electron energies to which the experiment is sensitive; however, Kahler (1974) and Peterson *et al.* (1973) have given evidence that the solar electron spectrum may at times extend down to 5 keV or below.

Historically the first question in energetics has been whether or not the nonthermal electrons have enough energy to provide the heating of the thermal flare plasma. This computation depends on assumptions about the ambient density of the hot flare plasma and about the low energy cutoff of the electron spectrum. Kahler and Kreplin (1971) and McKenzie *et al.* (1973) compared the two energetic quantities and found that nonthermal electrons do have sufficient energy to heat the plasma. For the OSO-7 hard X-ray events, the median thermal energy is $U=3\times10^{29}$ erg if a density of 5×10^{10} cm^{-3} is assumed. For a 20 keV electron spectrum cutoff, the median thin target and thick target collision losses were respectively 5×10^{27} erg and 2×10^{28} erg, which is insufficient; however, if a cutoff of 10 keV is assumed, the collision losses are increased by an order of magnitude and they become comparable to the plasma thermal energy. If, following the above mentioned authors, a 10 keV cutoff is adopted, then the nonthermal collision loss energy and the plasma thermal energy are comparable in magnitude.

Since the OSO-7 instrument simultaneously observes hard and soft X-ray spectra, it is possible to compare not only the total amounts of thermal and nonthermal energy, but also make a detailed time comparison of these forms of energy. Figure 8 gives such

a comparison. The top trace in the figure gives the product of the thermal energy of the flare plasma and the ambient density, obtained from the product of the observed temperature and emission measure, $Q = 3\, n_e n_i\, VkT = (3\, NkT) n_i$. Q is taken to be representative of the thermal energy input, which as stated earlier must be due to the addition of new hot material to the soft X-ray emitting region. If this region maintains a constant volume throughout the evolution (case 3), then Q will be proportional to

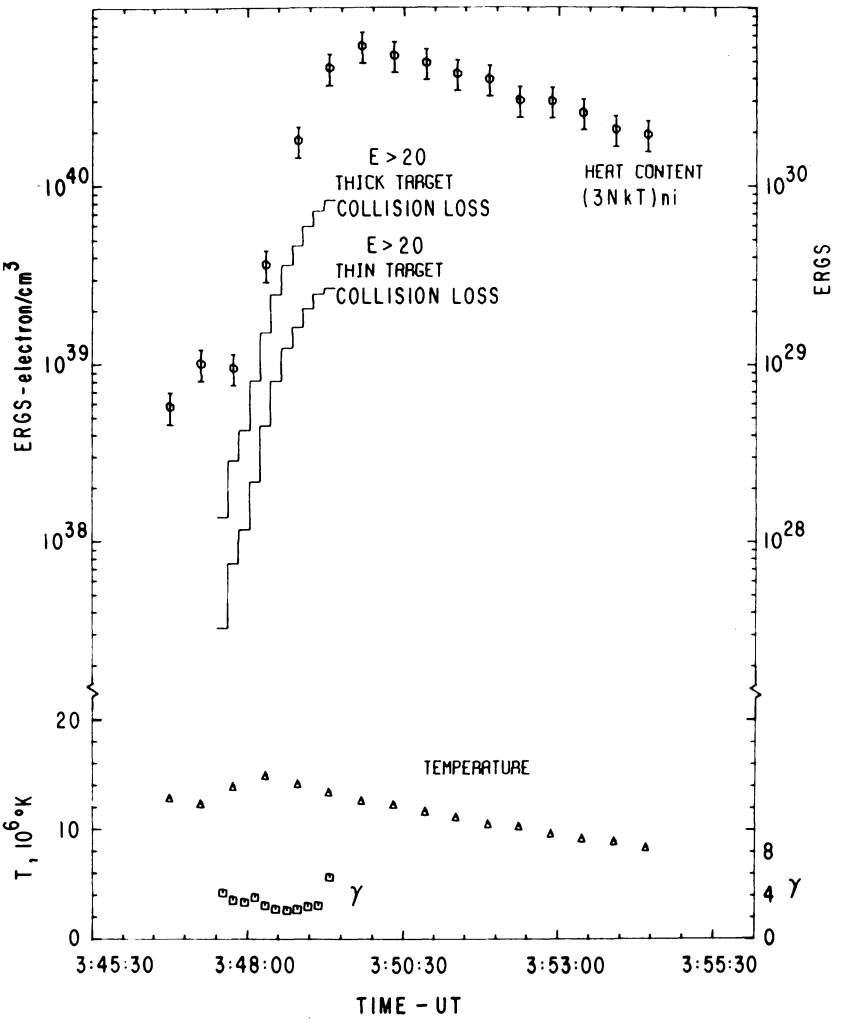

Fig. 8. Energetics of the sample X-ray burst in 1972, January 26. The top trace gives the heat content of the thermal plasma, the product of the total thermal energy and the ambient density. The peak value of this quantity is 6×10^{40} erg electron cm^{-3}, so that if the ambient density is assumed to be 5×10^{10} cm^{-3}, then the thermal energy is 1.2×10^{29} erg. The next two traces give the cumulative thick and thin target collision losses in ergs, which are the time integrals of the thick and thin target power. The triangles give the successive measurements of the temperature of the flare plasma, and the boxes give the values of the hard X-ray spectral exponent γ. Note that the input of nonthermal energy drops below threshold 30 s before the peak in Q.

https://doi.org/10.1017/S0074180900071692 Published online by Cambridge University Press

the square of the energy input, whereas for constant density (case 4) Q will be directly proportional to the thermal energy growth. The solid line traces the cumulative collision loss energy in both the thick and thin target approximations, $W = \Sigma P \Delta t$. The lowest two traces give the plasma temperature as derived from the soft X-rays and the spectral index of the hard X-rays, γ.

Figure 8 presents the comparison for the sample event of 1972, January 25. The growth of the quantity Q continues for 30 s after the end of the collisional energy input; this behavior is typical of the 123 events analyzed. This behavior is more strongly pronounced in the event of 1972, May 14 at 1504 UT, shown in Figure 9; in

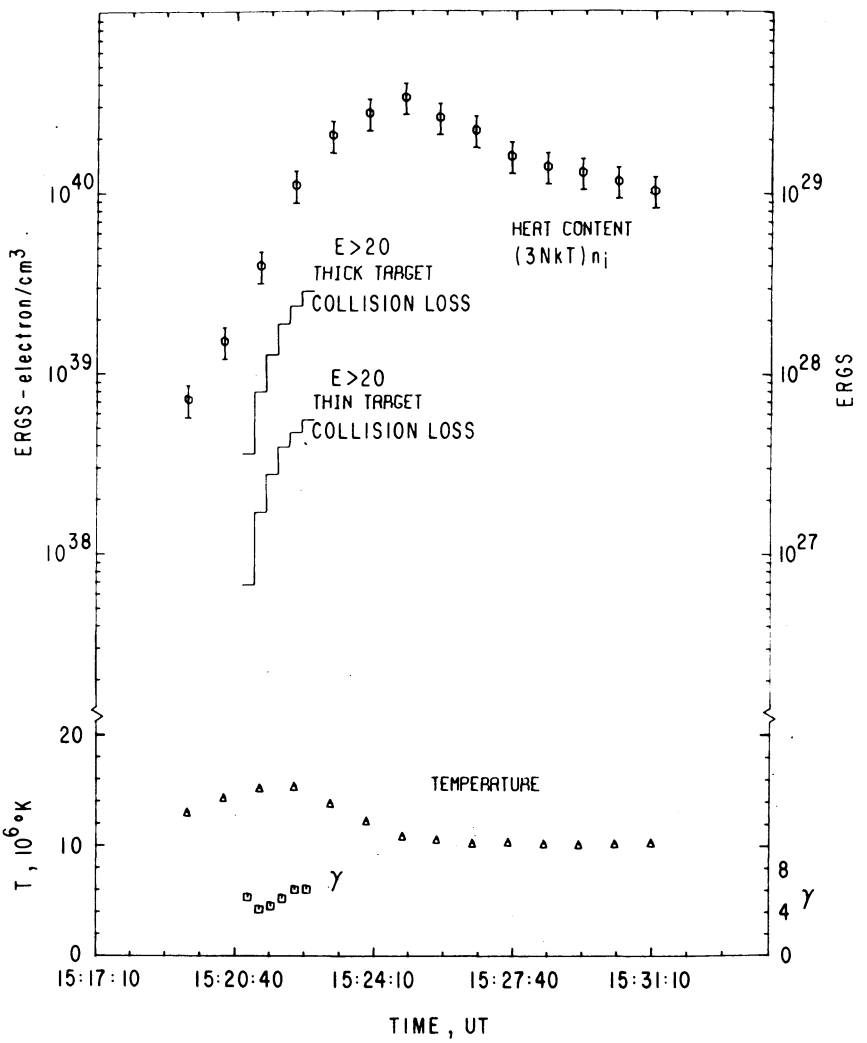

Fig. 9. The same as Figure 8, but for the event of 1972, May 14 at 1504 UT. When the nonthermal energy input had ceased, the heat content has reached only 25% of its largest value, which occurred 60 s later.

https://doi.org/10.1017/S0074180900071692 Published online by Cambridge University Press

this case the heat content Q attained only 25% of its final value when the collision losses were no longer detectable. This detailed comparison of the timing of the thermal and nonthermal energies in solar X-ray bursts indicates that the collision losses do not come at the correct time to directly energize the hot flare plasma. Thus an alternative plasma heating source is required. The existence of another energy source is also consistent with the fact that in one third of the soft X-ray bursts no hard X-rays are detected.

V. Center-to-Limb Effects

The study of longitude variations of solar X-ray emission is a powerful technique for examining the geometrical structure of X-ray emitting regions. For events on the visible disk of the sun, variations from center to limb will reveal any anisotropy which may be present in the emission. Occultation of the lower portions of a burst by the limb will give additional information about the spatial extent of the emitting regions.

In the soft X-ray region, Catalano and Van Allen (1973) successfully applied the technique of observing a burst with two spacecraft at different heliocentric longitudes: they determined the scale height for soft X-ray emission in the 2–12 Å band to be 1.1×10^4 km. Kreplin and Taylor (1971) used lunar occultation of an X-ray burst and measured its horizontal extent in the 1–8 Å band, 140000 km. Imaging experiments have also been flown (Vaiana *et al.*, 1973) to measure the sizes of soft X-ray emitting regions. In the hard X-ray region the only direct observation is that of Takakura *et al.* (1971); they used a modulation collimator to place a 1′ upper limit on the size of the X-ray source.

Evidence for the height of hard X-ray emission comes from the observations of Wood and Noyes (1972) indicating the EUV radiation is well correlated in time with nonthermal X-ray emission; they identified the origin of EUV emission to be heating by collision losses of the X-ray emitting electrons. Since the spectral lines observed were characteristic of ionic species found in the transition region, they concluded that the energetic electron collision losses were taking place at that level. Because of the high density, the thick target approximation is expected to be applicable. Vorpahl (1973), Hudson (1973), and Kane and Donnelley (1971) have all given evidence to support chromospheric thick target models. In these cases we would expect that since the height of emission is below 5000 km, X-ray emission from flares more than 7° beyond the limb could reach us only by scattering off of higher layers in the solar atmosphere, and thus would be strongly suppressed. Accordingly, no burst which is well behind the limb should give detectable hard X-ray fluxes.

On the other hand, hard X-ray emission from high in the corona has been reported. Frost and Dennis (1971) observed hard X-rays from the flare of 1969, March 30 which was far behind the limb. Datlowe and Lin (1973) have reported correlated observations of X-rays, type III bursts, and interplanetary electrons, which they interpret as good evidence for escaping electrons and X-ray emission high in the corona.

Thirty-seven OSO-7 soft X-ray bursts have been identified as having come from behind the limb of the Sun. The method of identification, described in detail in Roy

and Datlowe (1974), uses full-disk Hα pictures to select bursts with no accompanying optical counterpart and to track prolific bursts producing regions over the limb. Locations of over-the-limb bursts are estimated using the time of limb passage and the solar rotation rate. Of the 37 bursts, 24 (two-thirds) had a detectable hard X-ray component. This is the same fraction as exhibited by events near the center of the disk. Moreover, of the eight events with expected longitudes $\theta > 100°$, corresponding to minimum visible heights from 10^4–10^5 km, five had a detectable nonthermal component. This is entirely inconsistent with the chromospheric emission model or with any model of localized X-ray emission. At least some of the hard X-ray emission must therefore come from considerable heights in the corona, and the evidence supports the contention that the vertical distribution of this emission is similar to that of the soft X-ray emission.

For events on the solar disk, there is no center-to-limb variation in the relative frequency of either soft or hard X-ray bursts. Since the optical counterparts are used to identify the location of the X-ray bursts, the Hα longitude variation must be taken into account. To remove this effect the longitude distribution of the X-ray bursts was normalized by the longitude distribution of 2011 confirmed subflares reported during the observing period. The data were collected into three groups 0–29°, 30–59° and 60–87° longitude, with east and west summed together. No statistically significant longitude variation was found for either the hard or soft X-ray bursts. For the soft X-rays one standard deviation in each of the bins was respectively 13%, 13%, and 19%; the corresponding numbers for the hard X-rays were 19%, 19%, and 28%. Since the instrument operates at a fixed 20 keV threshold, these observations mean that there is no longitude variation in the intrinsic brightness of hard X-ray bursts, no limb brightening or darkening at 20 keV comparable to the effect seen in Hα.

In the hard X-ray spectra there is however a significant center-to-limb effect. Figure 10 shows the distribution of X-ray spectra at the time of maximum flux, γ_m, in a manner similar to Figure 7. In this case however the data have been divided into two groups, bursts occurring between $0 \leqslant \theta \leqslant 59°$ (upper part) and $\theta \geqslant 60°$ (lower part). The limb events are subdivided into the ones which occurred on the disk (shaded) and those which were beyond the limb (black). These two distributions differ principally in the region of small spectral index, $\gamma_m \leqslant 3.5$. The difference in the medians of the two distributions is $\Delta\gamma = 0.7$. Using the $\theta < 60°$ events as the reference distribution, the probability that the over-the-limb event distribution would occur by randomly choosing events is 6×10^{-3}; the probability that the limb event distribution would result from randomly choosing events from the reference distribution is 5×10^{-3}, and the equivalent number for the 62 events with $\theta \geqslant 60°$ is 8×10^{-4}. The difference in the two hard X-ray spectral distributions has a high degree of statistical significance.

One immediate consequence of these observations is that thermal interpretations of the hard X-ray emission from the Sun can be ruled out. Anisotropic emission from a thermal plasma can occur if the pitch angle distribution is highly anisotropic, but on the Sun the relaxation times should be quite short. Therefore no thermal plasma would be expected to yield the observed longitude effect.

There is at present no satisfactory quantitative model for the origin of the center-to-

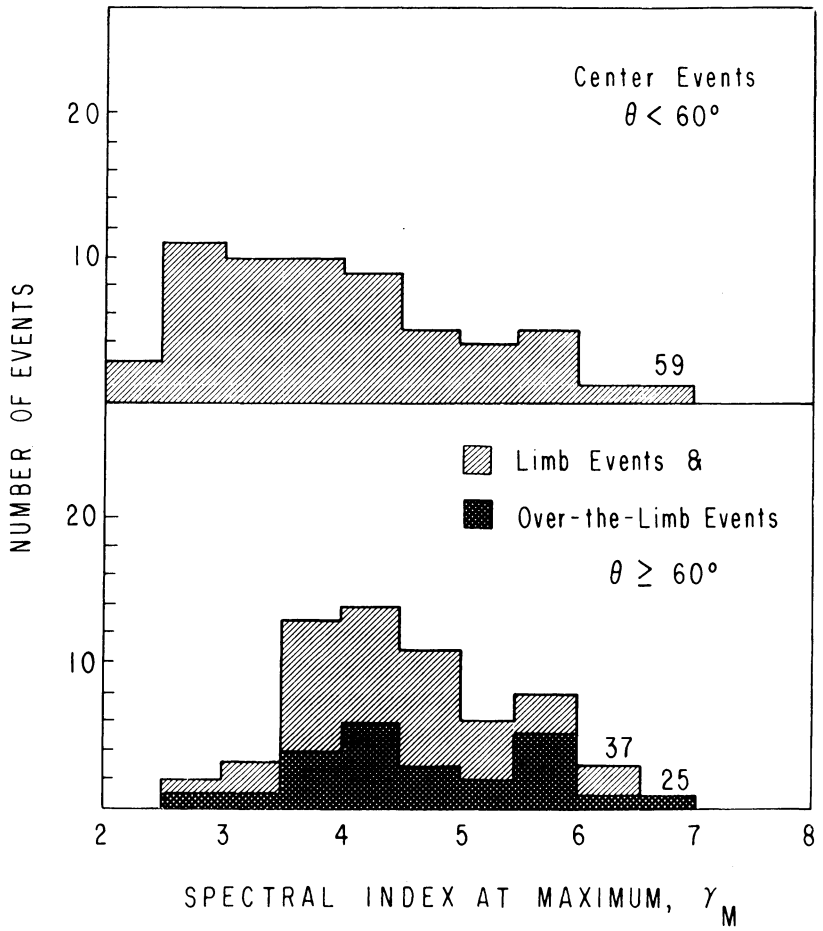

Fig. 10. Variation of spectral index at minimum with solar longitude. The upper panel gives the distribution of frequency of occurrence of γ_m for events associated with flares occurring at longitudes of 0–59°. The lower panel gives the same distribution for limb (60–87°) and over-the-limb events. The two distributions differ primarily in the absence of events in the range $2.5 \leqslant \gamma_m \leqslant 3.5$ in the $\theta \geqslant 60°$ group.

limb spectral variation. Occultation of an inhomogeneous source with spectra that soften with altitude cannot explain the effect, because it occurs on the disk as well as behind the limb. Compton backscattering of X-rays from the solar atmosphere (Tomblin, 1972) will produce a hardening of spectra from bursts near disk center at some energies, but according to the calculations of Santangelo *et al.* (1973), in the 20–50 keV energy range on which the OSO-7 spectra principally depend, the alteration of the spectral slope will be small. Thick target streaming models (Brown, 1972; Petrosian, 1973) predict a small variation of the spectrum with longitude but they also predict a large limb brightening which is not observed. None of these models gives a quantitative explanation of the origin of the effect.

https://doi.org/10.1017/S0074180900071692 Published online by Cambridge University Press

VI. Summary

The OSO-7 solar X-ray experiment has provided a wealth of new information about bursts. The principal results of the data analysis so far are the following:

(1) The growth of the soft X-ray emission in a burst must be due to the addition of new hot material to the flare plasma.

(2) The anticorrelation between the cooling time and the maximum plasma temperature gives new evidence to support conduction as the principal cooling mechanism of the hot flare plasma.

(3) Although nonthermal electrons may have sufficient energy to heat the flare plasma, the relative timing between hard and soft X-ray observations indicates that some other source of energy must also heat the plasma.

(4) The observations of hard X-ray emission from bursts which occurred behind the limb indicate that hard X-ray emission comes at least in part from considerable heights in the corona.

(5) The spectra of hard X-ray bursts which occur near or beyond the limb are significantly softer than those occurring near the center of the disk.

Acknowledgments

Professor Laurence Peterson of the University of California, San Diego, is the principal investigator for the OSO-7 Solar X-ray Experiment. D. L. McKenzie of the Aerospace Corp. played an important role in the design and construction of the instrument and in the early analysis of the data. This presentation would not have been possible without numerous valuable discussions with Hugh S. Hudson and Michael J. Elcan of UCSD. This work was supported under National Aeronautics and Space Administration Contract NAS-5-11081 and U.S. Air Force Contract F19628-74-C-0046.

References

Brown, J. C.: 1972, *Solar Phys.* **26**, 459
Catalano, C. P. and Van Allen, J. A.: 1973, *Astrophys. J.* **185**, 335.
Culhane, J. L..: 1969, *Monthly Notices Roy. Astron. Soc.* **144**, 375.
Culhane, J. L. and Acton, L. W.: 1970, *Monthly Notices Roy. Astron. Soc.* **151**, 141.
Culhane, J. L. and Phillips, K. J. H.: 1970, *Solar Phys.* **11**, 117.
Culhane, J. L., Vesecky, J. F., and Phillips, K. J. H.: 1970, *Solar Phys.* **15**, 394.
Datlowe, D. W. and Lin, R. P.: 1973, *Solar Phys.* **32**, 459.
Datlowe, D. W., Hudson, H. S., and Peterson, L. E.: 1974a, *Solar Phys.* **35**, 193.
Datlowe, D. W., Elcan, M. E., and Hudson, H. S.: 1974b, *Solar Phys.* **39**, 155.
Frost, K. J.: 1969, *Astrophys. J. Letters* **158**, L159.
Frost, K. J. and Dennis, B. R.: 1971, *Astrophys. J.* **165**, 655.
Horan, D. M.: 1971, *Solar Phys.* **21**, 188.
Hudson, H. S.: 1973, in R. Ramaty and R. G. Stone (eds.), *High Energy Phenomena on the Sun*, NASA SP-342, p. 207.
Hudson, H. S. and Ohki, K.: 1972, *Solar Phys.* **23**, 155.
Hudson, H. S., Peterson, L. E., and Schwartz, D. A.: 1969, *Astrophys. J.* **157**, 389
Kahler, S. W.: 1973, in R. Ramaty and R. G. Stone (eds.), *High Energy Phenomena on the Sun*, NASA SP-342, p. 124.

Kahler, S. W. and Kreplin, R. W.: 1971, *Astrophys. J.* **168**, 531.
Kahler, S. W., Meekins, J. F., Kreplin, R. W., and Bowyer, C. S.: 1970, *Astrophys J.* **162**, 293.
Kane, S. R.: 1974, in G. Newkirk, Jr. (ed.), 'Coronal Disturbances', *IAU Symp* **57**, 105.
Kane, S. R. and Anderson. K. A.: 1970, *Astrophys. J.* **162**, 1003.
Kane, S. R. and Donnelley, R. F.: 1971, *Astrophys. J.* **164**, 151.
Kreplin, R. W. and Taylor, R. G.: 1971, *Solar Phys.* **21**, 452.
McKenzie, D. L., Datlowe, D. W., and Peterson, L. E.: 1973, *Solar Phys.* **28**, 175.
Neupert, W. M.: 1967, *Solar Phys.* **2**, 294.
Peterson, L. E. and Winckler, J. R.: 1959, *J. Geophys. Res.* **64**, 1969.
Peterson, L. E., Datlowe, D. W., and McKenzie, D. L.: 1973, in R. Ramaty and R. G. Stone (eds.), *High Energy Phenomena on the Sun*, NASA-SP-342, p. 132.
Petrosian, V.: 1973, *Astrophys. J.* **186**, 291.
Roy, J. R. and Datlowe, D. W.: 1974, *Solar Phys.*, to be published.
Solar Geophysical Data, CRPL-FB 332-340, 1972.
Santangelo, N., Horstman, H., and Horstman-Moretti, E.: 1973, *Solar Phys.* **29**, 143.
Takakura, T., Ohki, K., Shibuya, N., Fujii, M., Matsuoka, M., Miyamoto, S., Nishimura, J., Oda, M., Ogawara, Y., and Ota, S.: 1971, *Solar Phys.* **16**, 454.
Teske, R. G.: 1971, *Solar Phys.* **19**, 356.
Tomblin, F. F.: 1972, *Astrophys. J.* **171**, 377.
Vaiana, G. S., Davis, J. M., Giacconi, R., Krieger, A. S., Silk, J. K., Timothy, A. F., and Zombeck, M.: 1973, *Astrophys. J. Letters* **185**, L47.
Valcinek, B., Farnik, F., Horn, J., Letfus, V., Sudova, J., Komarek, B., Engelthaler, P., Ulrych, J., Moucka, L., Fronka, O., Vasek, T., Beranek, I., Plch, J., and Zderadicka, J.: 1973, *Bull. Astron. Inst. Czech.* **24**, 362.
Vorpahl, J. A.: 1973, in R. Ramaty and R. G. Stone (eds.), *High Energy Phenomena on the Sun*, NASA SP-342, p. 221.
White, W. A.: 1964, in W. N. Hess (ed.), AAS-NASA Symposium on the *Physics of Solar Flares*, NASA SP-50, p. 131.
Wood, A. T. and Noyes, R. W.: 1972, *Solar Phys.* **24**, 180.